Pramana – J. Phys. (2019) 93:42
https://doi.org/10.1007/s12043-019-1807-2

A third-order memristive Wien-bridge circuit and its integrable deformation

BIRONG XU[1,2], GUANGYI WANG[1,*], XIAOYUAN WANG[1] and HERBERT HO-CHING IU[3]

[1]Institute of Modern Circuits and Intelligent Information, Hangzhou Dianzi University, Hangzhou 310018, China
[2]College of Mechanic and Electronic Engineering, Wuyi University, Wuyishan 354300, China
[3]School of Electrical, Electronic and Computer Engineering, The University of Western Australia, 35 Stirling Highway, Crawley, WA 6009, Australia
*Corresponding author. E-mail: wanggyi@163.com

MS received 25 October 2018; revised 13 February 2019; accepted 13 March 2019; published online 21 June 2019

Abstract. In this paper, a novel passive memristor model and its equivalent circuit model are designed, analysed and realised to investigate the memristor characteristics and their applications in nonlinear circuits. By employing this memristor model, a new third-order memristive Wien bridge is set up. Dynamical behaviours of the system are studied in detail, and multiscroll attractors, coexisting bifurcation modes, coexisting attractors, antimonotonicity and transient chaotic bursting are observed in this system by using theoretical analysis, simulation analysis and circuit experiment. Integrable deformation of the memristive Wien-bridge system is analysed. The circuit experiment is performed by replacing the memristor with its equivalent circuit model in the proposed memristor-based Wien-bridge circuit.

Keywords. Memristor; chaos; Wien-bridge circuit; integrable deformation.

PACS Nos 05.45.Ac; 05.45.Pq; 05.10.Aa

1. Introduction

The memristor, recognised as the fourth circuit element, was predicted by Chua [1] in 1971. In 2008, HP laboratory reported the implementation of a nanoscale memristor [2], which aroused wide interest in academia and industry. The research of memristors mainly focusses on physical implementation [2–6] and applications [7–11], and has achieved some results.

Nanoscale memristors that store information without the need for an internal power source can be used for non-volatile memories [7], neural networks [9], nonlinear circuits [10,11], digital logic circuits [12] and so on.

In the field of memristor-based chaotic circuits, Itoh and Chua [11] derived several memristive chaotic systems from Chua's oscillator by replacing Chua's nonlinear resistor with a piecewise-linear memristor, which has greatly stimulated the study on memristor-based chaotic circuits. Afterwards, some memristive Wien bridges are constructed in refs [13–17]. Li and Zeng [13] employed a piecewise-linear memristor to construct a fourth-order memristor-based Wien-bridge circuit, which can generate chaotic and hyperchaotic behaviours. Yu *et al* [14] introduced a generalised memristor into a Wien-bridge oscillator to establish a fifth-order chaotic circuit. Wu *et al* [15] constructed an active generalised memristor, with which a fourth-order Wien-bridge chaotic oscillator was designed further. By employing a flux-controlled memristor to replace the resistance of a fourth-order Wien-bridge circuit, Ye *et al* [16] built a fifth-order Wien-bridge hyperchaotic circuit. Although these memristive Wien-bridge systems are chaotic or hyperchaotic circuits, which have rich dynamical behaviours, these chaotic systems are high-order chaotic circuits, i.e. of the fourth or the fifth order, which makes it difficult to analyse and design. Bao *et al* [17] proposed a third-order memristive oscillator, exhibiting symmetric periodic bursting, but the memristive circuit does not show chaotic behaviour. Moreover, all these memristive Wien bridges are based on the canonical Wien bridge. To explore a chaotic circuit combining a memristor and a non-canonical Wien bridge, we design a third-order memristive chaotic system based on a non-canonical Wien bridge and a passive memristor model. The proposed Wien-bridge chaotic system can generate a multiscroll chaotic attractor, and

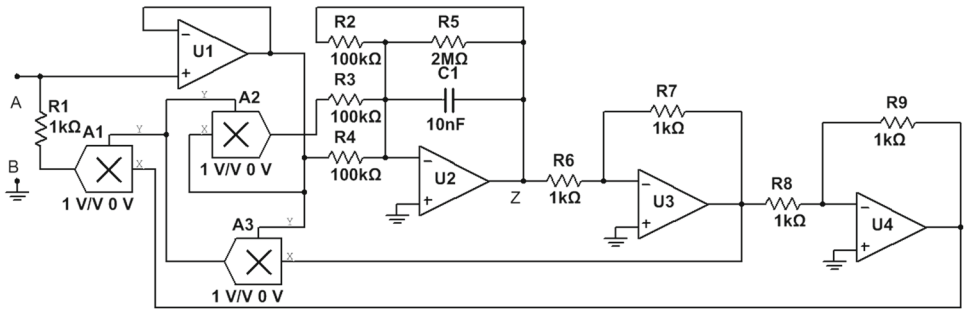

Figure 1. Equivalent circuit of the memristor.

exhibits some complex dynamical characteristics, such as coexisting bifurcation modes, coexisting attractors, antimonotonicity and transient chaotic bursting. As the system possesses complex dynamical behaviours, it can be employed in information engineering, e.g. the generation of pseudorandom sequences in various information encryptions. In addition, the integrable deformation of the Wien-bridge chaotic system is analysed.

2. A memristive non-canonical Wien-bridge system

2.1 *A memristor model and its equivalent circuit*

Memristor was proposed by Chua [1] in 1971, and after that, Chua and Kang [18] generalised the definition of the memristor as follows:

$$y(t) = M(z, u, t)u(t),$$
$$\frac{\mathrm{d}z}{\mathrm{d}t} = F(z, u, t), \tag{1}$$

where $u(t)$ and $y(t)$ are the input and output of a memristor, respectively, and z is the state variable of a system. $F(\cdot)$ and $M(\cdot)$ are differentiable scalar-valued functions, which are related to the specific device.

To design a third-order memristive Wien bridge-based system, we introduce a voltage-controlled memristor, and the internal state function is set as $\mathrm{d}z/\mathrm{d}t = -v_\mathrm{M} - hz + v_\mathrm{M}^2 z$, where v_M denotes the voltage across the memristor. The voltage-controlled memristor employed in a Wien bridge-based system should be a passive memristor, thereby its memductance is set as $W(z) = \gamma(z^2 + \beta)$. The sign before the parameter β denotes polarity. If the sign is '+', the memristor is a passive element. Otherwise, the memristor is active. For simplifying the expression of the chosen memristor, let $\gamma = c$ and $\gamma\beta = 1$. Hence, the memristor is expressed as

$$i_\mathrm{M} = (1 + cz^2)v_\mathrm{M},$$
$$\frac{\mathrm{d}z}{\mathrm{d}t} = -v_\mathrm{M} - hz + v_\mathrm{M}^2 z, \tag{2}$$

where i_M is the current passing through the memristor.

To further explore the memristor, we designed its equivalent circuit, as shown in figure 1. From the equivalent circuit, we get

$$i_\mathrm{M} = \frac{1}{R_1}\left(1 + \frac{R_9}{R_8}z^2\right)v_\mathrm{M},$$
$$\frac{\mathrm{d}z}{\mathrm{d}t} = \frac{1}{R_4 C_1}\left(-v_\mathrm{M} - \frac{R_4}{R_2}z + \frac{R_4}{R_3}v_\mathrm{M}^2 z\right). \tag{3}$$

When resistors and capacitors of the circuit are chosen as in figure 1, the input port AB connects to a sinusoidal voltage signal of amplitude $v_\mathrm{m} = 1$ V. In the sinusoidal excitation, the v–i characteristic of the memristor is shown in figure 2, which exhibits a pinched hysteresis loop and shows the most common of all memristors, ideal or otherwise. As shown in figure 2, the pinched hysteresis loops depend on the frequencies of the input signal, and the lobe area decreases as the frequency increases.

The memristor can be attributed to two types. One type is an active memristor, whose v–i characteristic curves exist in the first and the third quadrants. The other type is a passive memristor, of which the characteristic curves are in the second and the fourth quadrants. Figure 2 shows that the characteristic curves exist in the first and the third quadrants, and thus the proposed memristor is a passive memristor.

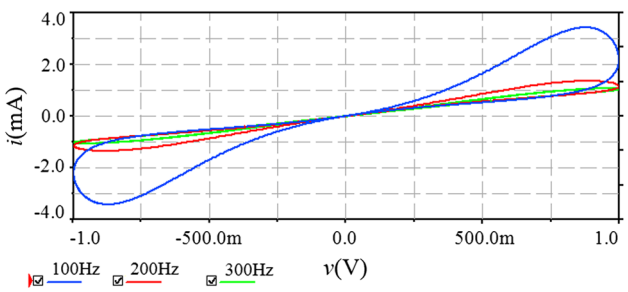

Figure 2. v–i hysteresis loops of the memristor.

2.2 *Model of a memristive Wien bridge-based system*

Employing the above memristor, a third-order memristive chaotic circuit based on the Wien bridge is proposed as shown in figure 3.

According to Kirchhoff's law and the relationship between the voltage and current of the elements, simultaneously considering eq. (2), the state equations of the circuit are obtained as

$$\begin{cases} C_1 \dfrac{\mathrm{d}v_1}{\mathrm{d}t} = \dfrac{(R_1/R_2)v_1 - v_2}{R_3} - (1 + cz^2)v_1, \\ C_2 \dfrac{\mathrm{d}v_2}{\mathrm{d}t} = \dfrac{(R_1/R_2)v_1 - v_2}{R_3}, \\ \dfrac{\mathrm{d}z}{\mathrm{d}t} = -v_1 - hz + v_1^2 z. \end{cases} \tag{4}$$

Let $v_1 = x$, $v_2 = y$, $R_1/R_2R_3C_1 = R_1/R_2R_3C_2 = a$, $1/R_3C_1 = 1/R_3C_2 = b$ and $1/C_1 = 1$. Equation (4) can be expressed as

$$\begin{cases} \dfrac{\mathrm{d}x}{\mathrm{d}t} = (ax - by) - (1 + cz^2)x, \\ \dfrac{\mathrm{d}y}{\mathrm{d}t} = ax - by, \\ \dfrac{\mathrm{d}z}{\mathrm{d}t} = -x - hz + x^2 z. \end{cases} \tag{5}$$

For $a = 3.05$, $b = 1$, $c = 0.5$ and $h = 2$, and the initial condition taken as $(0, 1, 0)$, the Lyapunov exponents of the system are calculated as $\mathrm{LE}_1 = 0.028$, $\mathrm{LE}_2 = 0$, $\mathrm{LE}_3 = -0.406$ and the corresponding Lyapunov dimension is $D_\mathrm{L} = 2.069$. These indicate that the system is a chaotic oscillator under proper parameters. Figure 4 shows the chaotic attractor, in which figure 4d depicts a four-scroll attractor. The corresponding Poincaré mappings on $z = 0$ are demonstrated in figure 5.

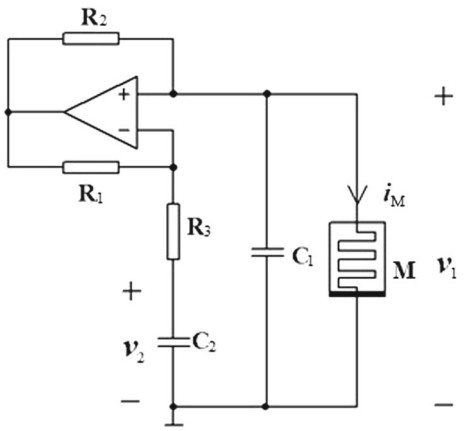

Figure 3. Memristive Wien-bridge circuit.

3. Characteristic analysis of the system

3.1 *Equilibrium point*

The divergence of eq. (5) is written as

$$\nabla V = \frac{\partial \dot{x}}{\partial x} + \frac{\partial \dot{y}}{\partial y} + \frac{\partial \dot{z}}{\partial z} = a - (1 + z^2) - b - h + x^2. \tag{6}$$

Obviously, if $\nabla V < 0$, the system is dissipative, and its attractor might be a chaotic attractor. System (5) is invariant under the coordinate transformation

$$(x, y, z) \to (-x, -y, -z). \tag{7}$$

It implies that this system is symmetrical about the original point. The left-hand side of eq. (5) is set to zero to obtain the equilibrium of system (5), written as

$$\begin{cases} ax - by - (1 + cz^2)x = 0, \\ ay - bx = 0, \\ -x - hz + x^2 z = 0. \end{cases} \tag{8}$$

Obviously, the system has a unique equilibrium $O(0, 0, 0)$, which differs from other memristive Wien-bridge chaotic systems that have line equilibrium or multiple equilibria. By linearising system (5) at the equilibrium, the Jacobian matrix is expressed as

$$J = \begin{bmatrix} a - 1 & -b & 0 \\ a & -b & 0 \\ -1 & 0 & -h \end{bmatrix}. \tag{9}$$

The corresponding characteristic equation is written as

$$F(\lambda) = [\lambda^2 - (a - b - 1)\lambda + b](\lambda + h) = 0. \tag{10}$$

The eigenvalues of the equilibrium are solved as

$$\begin{aligned} \lambda_1 &= -h, \\ \lambda_2 &= \frac{(a - b - 1)}{2} + \frac{1}{2}\sqrt{(a - b + 1)^2 - 4b}, \\ \lambda_3 &= \frac{(a - b - 1)}{2} - \frac{1}{2}\sqrt{(a - b + 1)^2 - 4b}. \end{aligned} \tag{11}$$

It shows that the equilibrium is asymptotically stable when $h > 0$ and $a < b + 1$, which is $\lambda_1 < 0$, $\mathrm{Re}(\lambda_2) < 0$ and $\mathrm{Re}(\lambda_3) < 0$. However, for $a = 3.05$, $b = 1$, $c = 0.5$ and $h = 2$, the eigenvalues are $\lambda_1 = -2$, $\lambda_2 = 0.525 + \mathrm{j}2.626$, $\lambda_3 = 0.525 - \mathrm{j}2.626$. λ_1 is a negative real root, while λ_2 and λ_3 are a pair of conjugate complex roots with a positive real part. Therefore, the equilibrium is an unstable saddle focus.

3.2 *The impacts of system parameters*

Now we explore the influence of parameters on the dynamical behaviours of the system. When we fix $b = 1$,

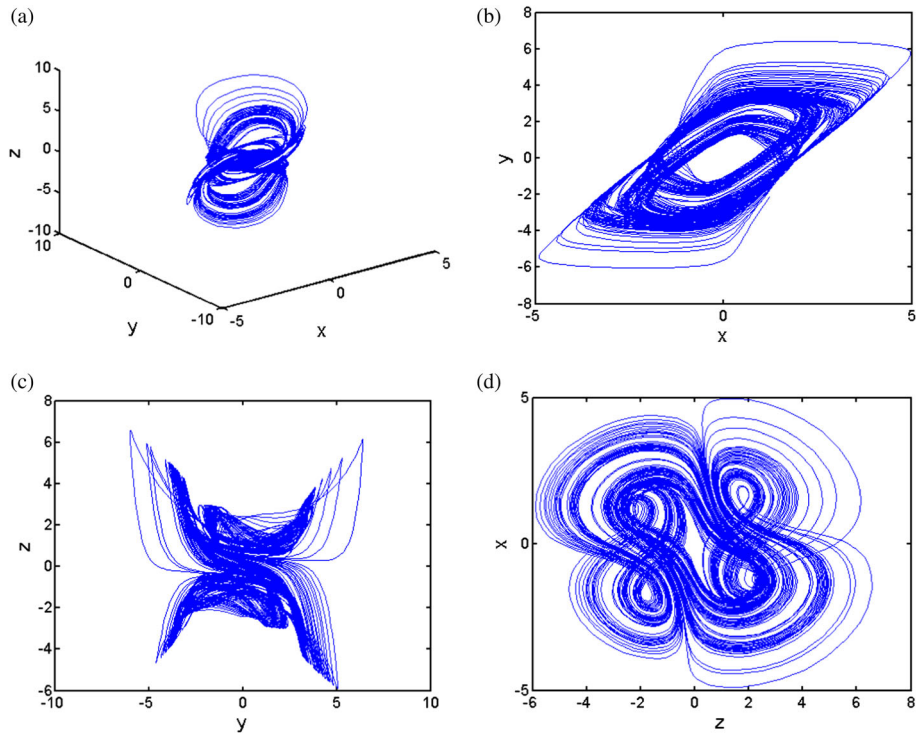

Figure 4. Chaotic attractors of the system: (**a**) x–y–z phase diagram, (**b**) x–y phase diagram, (**c**) y–z phase diagram and (**d**) z–x phase diagram.

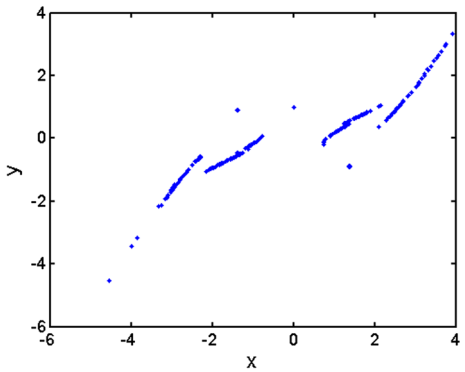

Figure 5. Poincaré mappings of the system on the $z = 0$ plane.

$c = 0.5$ and $h = 2$, and vary a from 2.5 to 3.3, with the initial condition as (0, 1, 0), the bifurcation diagram and the corresponding Lyapunov exponent spectra are obtained as shown in figures 6a and 6b, respectively. This dynamic process includes periodic windows, quasiperiodic and chaotic orbits. The system starts from the period-1 state, and it jumps into a chaotic state when a is about 2.515. In succession, several periodic windows appear in the chaotic region. Then, the system returns to a period-3 state when a is about 3.255. Particularly, if we take $a = 2.5$, 2.6 and 3.27, figures 7a–7c show periodic, quasiperiodic and chaotic attractors, respectively.

Setting $a = 3.05, c = 0.5, h = 2$ and $b \in [0.2, 2]$, the bifurcation diagram and the Lyapunov exponent spectrum are illustrated in figures 8a and 8b, respectively. Similarly, it is obvious that the system has complex dynamical behaviours on increasing the parameter b.

A dynamical map is displayed in figure 9 to investigate a and b influencing the states of the system simultaneously, in which the yellow regions represent the periodic states, the blue regions represent the chaotic states and the brown regions represent the unbounded states.

3.3 *Coexisting attractors and coexisting bifurcation modes*

Coexisting attractors and coexisting bifurcation modes discovered in refs [19–21] are special nonlinear phenomena, and became research hotspots recently. When the parameters are set as $a = 2.765$, $b = 1$ and $c = 1$, while h varies from 0.1 to 1.3, under the initial conditions (0, 1, 0) and (0, −1, 0), the coexisting attractors are found, as shown in figure 10. The orbits starting from the initial condition (0, 1, 0) are coloured blue, and the orbits starting from the initial condition (0, −1, 0) are coloured red. Under the two initial conditions, figures 10a and 10b

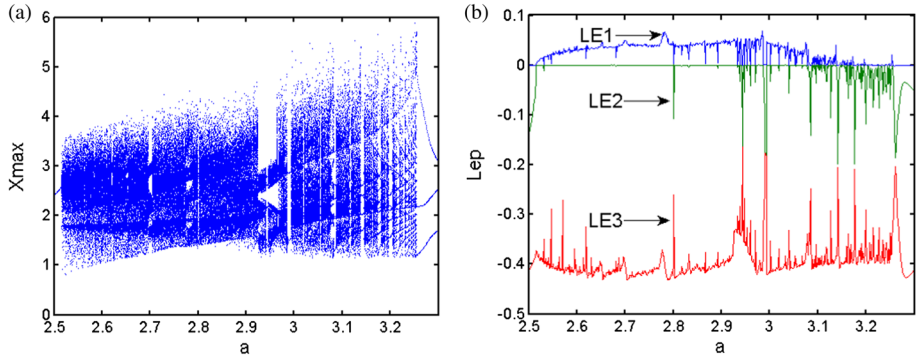

Figure 6. Bifurcation diagram and Lyapunov exponent spectrum with a changing from 2.5 to 3.3: (**a**) bifurcation diagram and (**b**) Lyapunov exponent spectrum.

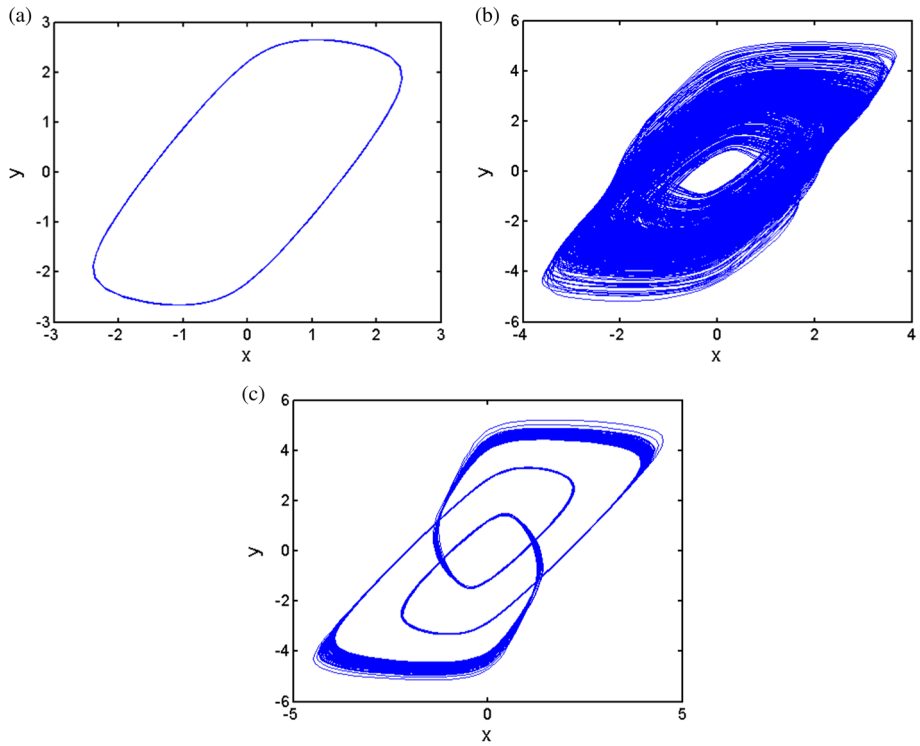

Figure 7. Phase diagrams on the x–y plane: (**a**) $a = 2.5$, (**b**) $a = 2.6$ and (**c**) $a = 3.27$.

display the coexistence of two period-1 attractors and two period-2 attractors with $h = 0.1$ and 0.2, respectively. When $h = 0.3$, the coexistence of the chaotic attractors is demonstrated in figure 10c, when $h = 0.4$ and 0.9, the coexistence of two quasiperiodic attractors is depicted in figures 10d and 10f. Furthermore, when $h = 0.5$ and 1.3, two ordinary chaotic attractors are observed in figures 10e and 10h, while for $h = 1.1$, two conventional quasiperiodic attractors are observed in figure 10g. Hence, there are numerous coexisting periodic, quasiperiodic and chaotic attractors in the system, as well as some conventional attractors that appear alternately with the coexisting attractors with increasing h, thereby implying the complexity of the system.

The attractive basin, which shows the multistability nature of nonlinear systems, is an important method to analyse coexistent attractors. Figure 11 gives the attractive basin in the cross-section of $a = 2.765$, $b = 1$, $c = 1$, $h = 0.3$ and $z(0) = 0$. It can be observed that there exist four different colours in the attractive basin, implying four different types of attractors in the given value region.

The coexisting bifurcation modes always accompany with the coexisting attractors phenomenon. Under the

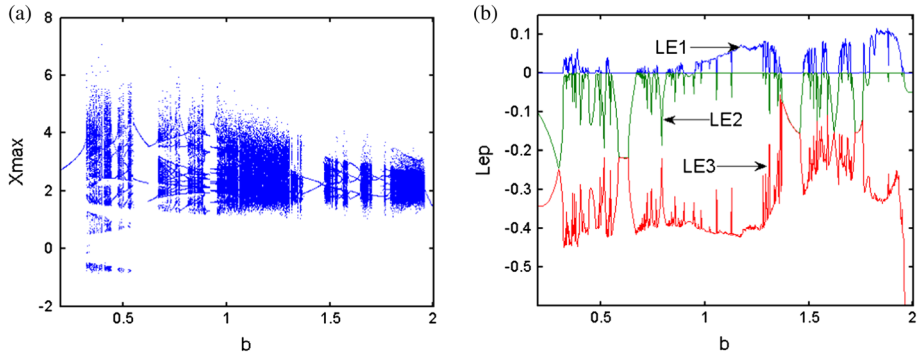

Figure 8. Bifurcation diagrams with b changing from 0.2 to 2: (**a**) bifurcation diagram and (**b**) Lyapunov exponent spectrum.

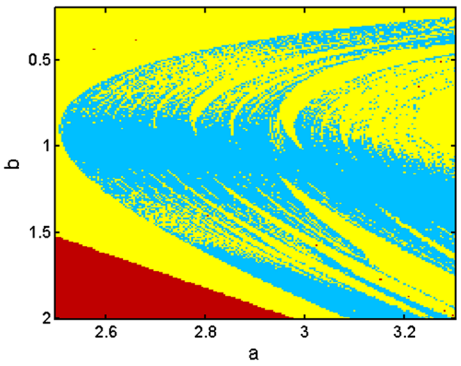

Figure 9. Dynamical map with a and b.

above parameters and initial conditions, the bifurcation diagram and the Lyapunov exponent spectrum are shown in figure 12. The Lyapunov exponent spectrum agrees with the bifurcation diagram very well, and the coexisting bifurcation modes are depicted. In the bifurcation diagram, there are forward and reverse period-doubling bifurcations and jump phenomenon.

3.4 *Variety of the chaotic attractors*

The proposed system can not only produce a four-scroll attractor on the z–x plane as shown in figure 4d, but also generate a double-scroll attractor and a one-scroll attractor. Setting the parameters as $a = 2.78$, $b = 1$, $c = 1$ and $h = 0.3$, with the same initial conditions as in §2.2, the double-scroll attractor is obtained, which is presented in figure 13a. If we choose $a = 2.76$, and other parameters are fixed, the coexisting one-scroll attractors are depicted in figure 13b. The blue one comes from the initial condition of (0, 1, 0), and the other initial condition is (0, −1, 0). Therefore, the scroll number of the attractor can be controlled by choosing the parameters.

Moreover, for the parameters $a = 2.8$, $b = 1$, $c = 1$ and $h = 0.3$, if the fourth-order Runge–Kutta method is employed to solve eq. (5), and 4000 steps are taken, figure 14a demonstrates the coexisting attractors. The red attractor starts from the initial condition of (0, 0.1, 0) and the blue one starts from the initial condition of (0, −0.1, 0). However, if 6000 steps are taken, the attractor from the former initial condition is displayed in figure 14b, which is a double-scroll attractor, but the two scrolls are different in density. Therefore, the coexisting one-scroll attractors do not exist for a long time.

3.5 *Antimonotonicity*

Antimonotonicity is a phenomenon of creation and annihilation of periodic orbits, which has been observed in some nonlinear systems, such as the memristive jerk system, memristive twin-T oscillator and the laser systems [22–24]. However, the phenomenon of antimonotonicity is never observed in memristive Wien-bridge oscillators, whereupon we investigate this phenomenon in our system. To illustrate this phenomenon clearly, some bifurcation diagrams of the parameter h are shown in figure 15, where the parameter b has some discrete values. From figure 15, we observe a primary bubble observed at $b = 0.96$, and a period-4 bubble at $b = 0.89$. For $b = 0.882$, a period-6 bubble appears. As b is further decreased, a Feigenbaum remerging tree (like chaos) occurs at $b = 0.8745$.

3.6 *Chaotic bursting and chaotic transient phenomena*

Bursting oscillation is a complex nonlinear behaviour, which is employed for communication in biological neurons [25,26]. In the past few years, this phenomenon has been discovered in many chaotic systems [15,27,28]. Some dynamical systems with two time scales can generate a combination of large-amplitude and small-amplitude oscillations. The system is considered to be in a quiescent state when the oscillation amplitude is zero or small. In contrast, when the oscillation amplitude is large, the system is in the spiking state. Bursting is the phenomenon of alternations between quiescent states and spiking states. Chaotic bursting is a type of

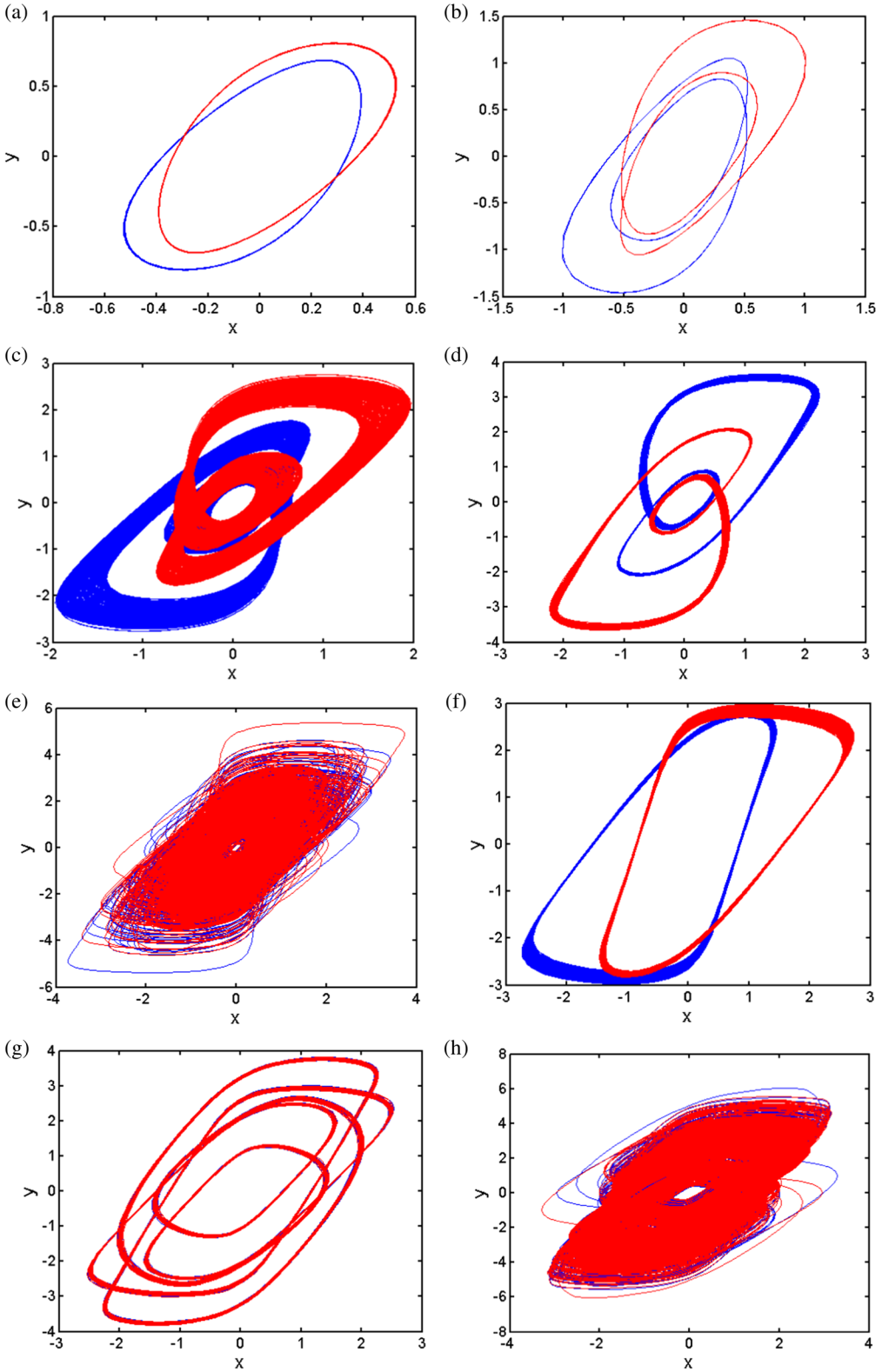

Figure 10. Attractors on the x–y plane with different h under initial conditions (0, 1, 0) (blue) and (0, −1, 0) (red): (**a**) coexisting period-1 attractors with $h = 0.1$, (**b**) coexisting period-2 attractors with $h = 0.2$, (**c**) coexisting chaotic attractors with $h = 0.3$, (**d**) coexisting quasiperiodic attractors with $h = 0.4$, (**e**) conventional chaotic attractors with $h = 0.5$, (**f**) coexisting quasiperiodic attractors with $h = 0.9$, (**g**) conventional quasiperiodic attractors with $h = 1.1$ and (**h**) conventional chaotic attractors with $h = 1.3$.

bursting pattern, whose oscillations are aperiodic. The chaotic bursting has been frequently exhibited in various kinds of neuronal models, and exists in some chaotic systems [29,30]. When the system has two time scales, the fast variables are modulated by the slow variable, leading to the emergence of bursting.

Hence, a system, which has a bursting phenomenon, can be divided into fast and slow subsystems such that the slow subsystem includes a single slow variable, and the fast subsystem includes the remaining variables, which are relatively fast [31]. The fast subsystem of system (5) is expressed as

$$\begin{cases} \frac{dx}{dt} = (ax - by) - (1 + cz^2)x, \\ \frac{dy}{dt} = ax - by, \end{cases} \tag{12}$$

which consists of the first and second equations in eq. (5), while the slow subsystem is expressed as

$$\frac{dz}{dt} = -x - hz + x^2 z, \tag{13}$$

which is the third equation of eq. (5). For the fast subsystem, the variable z can be considered as a conventional parameter, and its equilibrium point is obtained as $O(0, 0)$. The corresponding Jacobian matrix is expressed as

$$J_{\text{sub}} = \begin{bmatrix} a - (1 + cz^2) & -b \\ a & -b \end{bmatrix}. \tag{14}$$

Therefore, the characteristic equation is expressed as

$$\det(\lambda I - J_{\text{sub}}) = \lambda^2 + [b - a + (1 + cz^2)]\lambda + b(1 + cz^2). \tag{15}$$

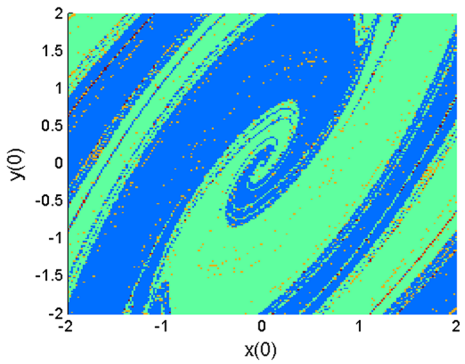

Figure 11. Attractive basins in the cross-section of $a = 2.765$, $b = 1$, $c = 1$, $h = 0.3$ and $z(0) = 0$.

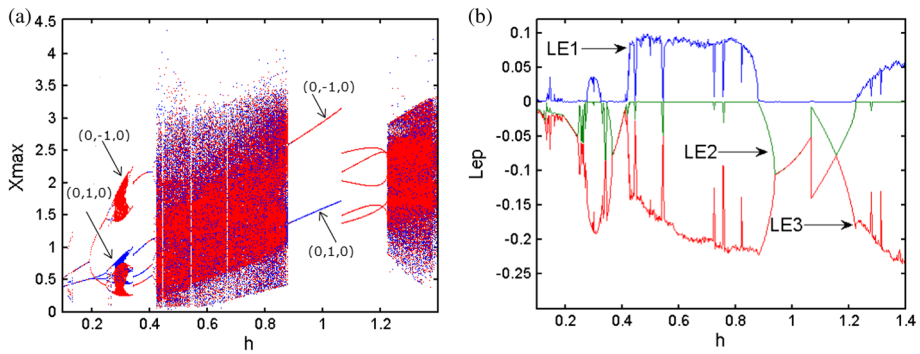

Figure 12. Coexisting bifurcation mode and Lyapunov exponent spectrum with respect to h under different initial conditions: (**a**) bifurcation diagram under initial conditions (0, 1, 0) (blue) and (0, −1, 0) (red) and (**b**) Lyapunov exponent spectrum.

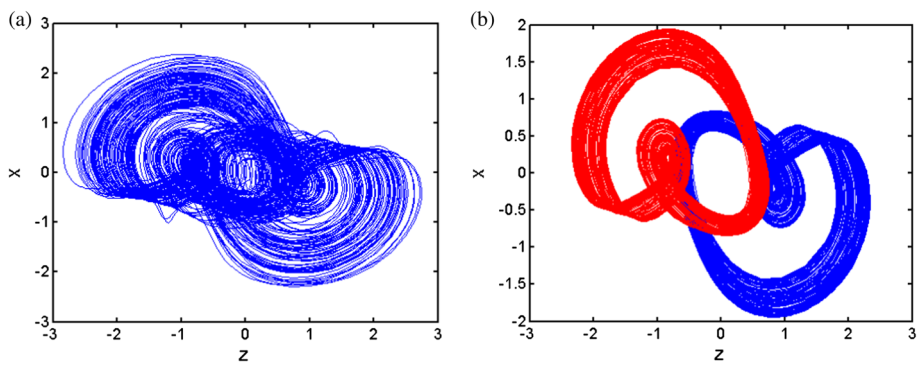

Figure 13. Attractors of different scroll number: (**a**) double-scroll attractor with $a = 2.78$ and (**b**) coexisting one-scroll attractors with $a = 2.76$.

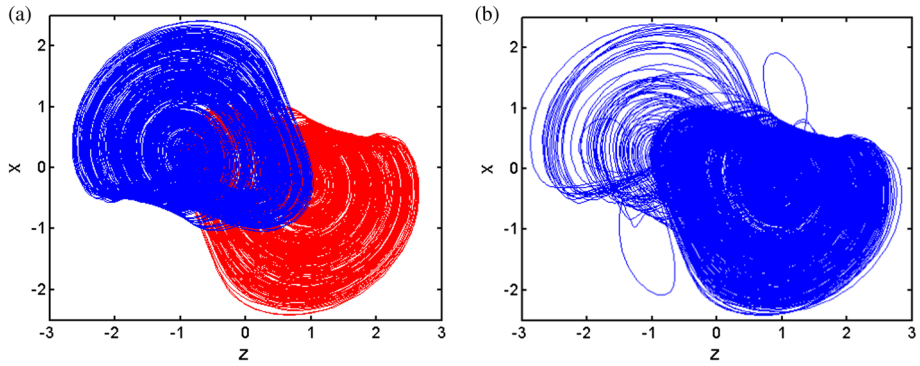

Figure 14. Attractors of different scroll numbers under different steps: (**a**) transient coexisting one-scroll attractors under 4000 steps and (**b**) double-scroll attractor under 6000 steps.

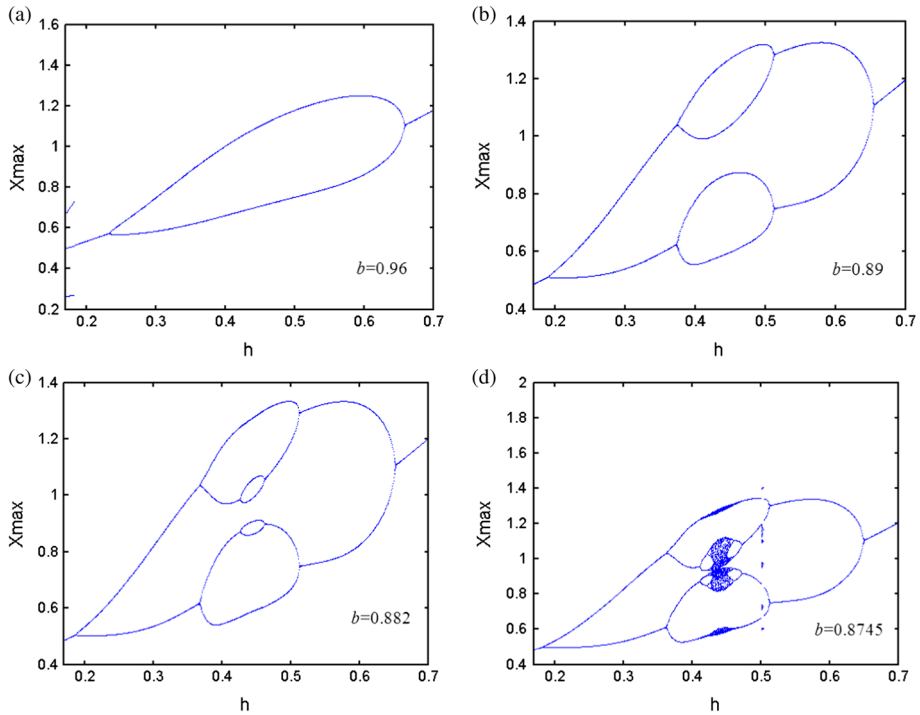

Figure 15. Bifurcation diagrams in terms of h: (**a**) a primary bubble at $b = 0.96$, (**b**) a period-4 bubble at $b = 0.89$, (**c**) a period-6 bubble at $b = 0.882$ and (**d**) a Feigenbaum remerging tree at $b = 0.8745$.

For $b > 0$ and $c > 0$, the solution of eq. (15) is non-zero, implying that fold bifurcation does not exist in system (5). As the Hopf bifurcation is associated with the existence of a pair of pure imaginary eigenvalues, the critical condition at the Hopf bifurcation point is $z = \pm\sqrt{(a - b - 1)/c}$.

When the parameters are selected as $a = 20$, $b = 0.5$, $c = 1$ and $h = 0.01$, with the initial conditions of (0.1, 0.1, −4.0) and (−0.1, −0.1, −4.0), the critical condition is $z = \pm 4.30$. By simulating, bursting oscillations appear as shown in figure 16, in which the variable $x(t)$ changes fast with time t, whereas the variable $z(t)$ is slow. The fast variable $x(t)$ is modulated by the low variable $z(t)$. Furthermore, both burstings are symmetric, of which the red one depends on the critical value $z = 4.30$ and the other relates to the critical value $z = -4.30$. Hence, we can conclude that the generation of the symmetric bursting oscillation is linked to the symmetric Hopf–Hopf bifurcation. From figure 16, it is clear that the bursting oscillations are aperiodic, indicating chaotic bursting.

However, this chaotic bursting is transient. For the initial condition of (0.1, 0.1, −4.0), the time-domain waveforms of $x(t)$ are shown in figure 17a, and the Lyapunov exponent spectrum is displayed in figure 17b. The

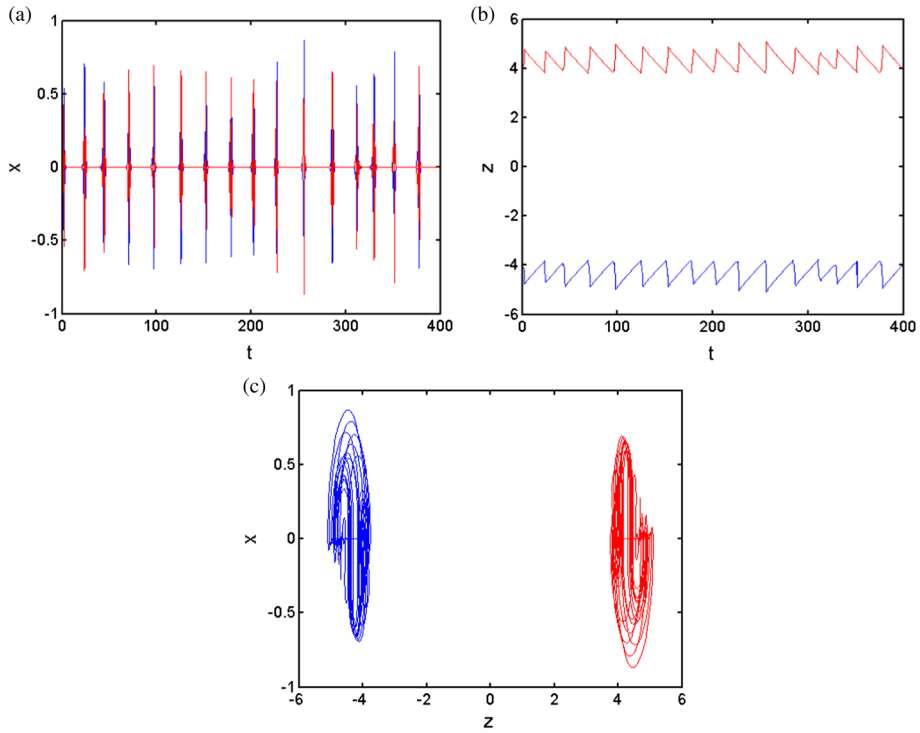

Figure 16. Time-domain waveforms and phase diagrams of chaotic bursting with the initial conditions of (0.1, 0.1, −4.0) (blue) and (−0.1, −0.1, 4.0) (red): (**a**) the time-domain waveforms of $x(t)$, (**b**) the time-domain waveforms of $z(t)$ and (**c**) z–x phase diagram.

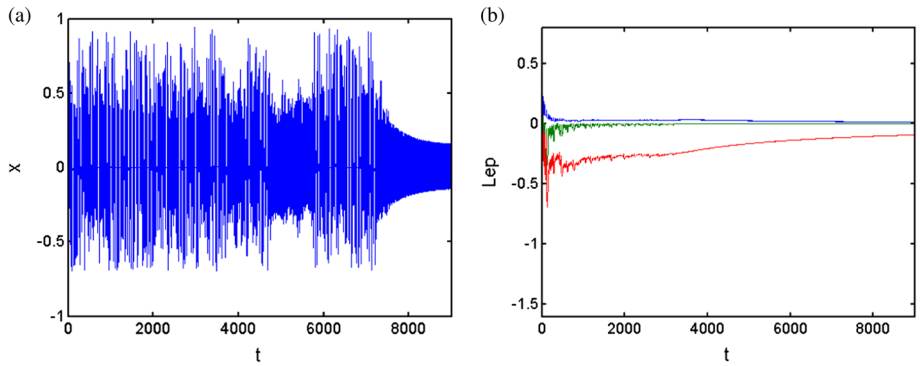

Figure 17. Transient chaotic bursting: (**a**) the time-domain waveforms of $x(t)$ and (**b**) the Lyapunov exponent spectrum.

Lyapunov exponent spectrum matches with the time-domain waveforms. From figure 16b, it can be seen that the largest Lyapunov exponent decreases to zero with time evolution.

4. Integrable deformation of the memristive Wien-bridge system

Chaotic systems can be applied in many fields. Thus, the construction of new chaotic systems has always been of concern. Lăzureanu proposed a novel method called the integrable deformation method to generate some new chaotic systems [32]. However, Lăzureanu [32] did not investigate the integrable deformation of a chaotic system with multistability. Therefore, due to its multistability, the integrable deformation of the memristive Wien-bridge system is investigated. The memristive Wien-bridge system $f(\mathbf{x})$ is assumed to consist of a Hamilton–Poisson part $g(\mathbf{x})$ and a non-conservative part $h(\mathbf{x})$. Note that the Hamilton–Poisson part is not unique, which is selected as

$$\begin{cases} \dfrac{\mathrm{d}x}{\mathrm{d}t} = -ay, \\ \dfrac{\mathrm{d}y}{\mathrm{d}t} = ax, \\ \dfrac{\mathrm{d}z}{\mathrm{d}t} = 0 \end{cases} \tag{16}$$

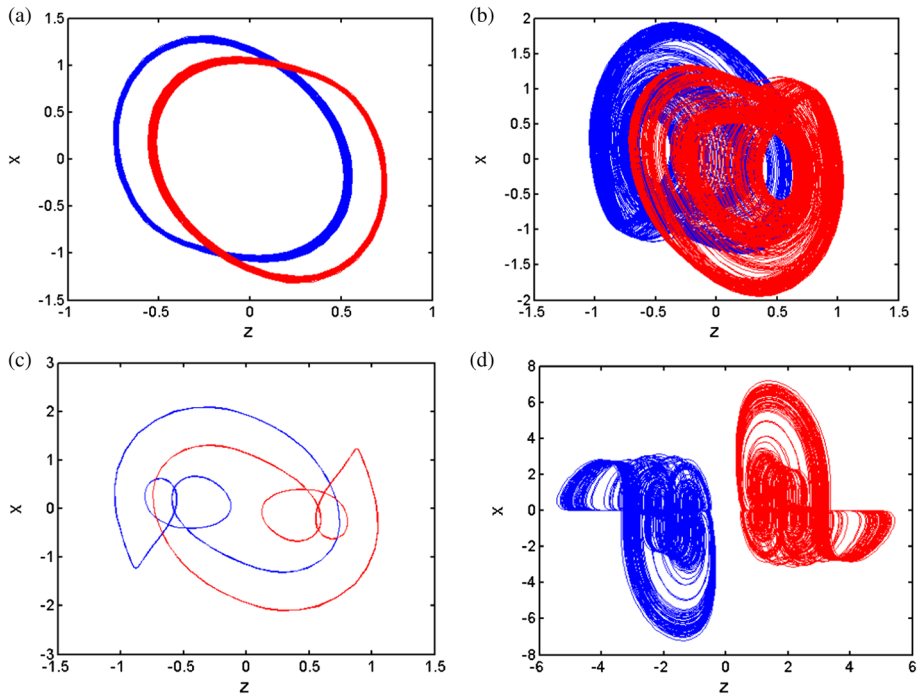

Figure 18. Coexisting attractors of the deformed system on the z–x plane with different a under initial conditions (0, 1, 0) (blue) and (0, −1, 0) (red): (**a**) coexisting quasiperiodic attractors with $a = 3.28$, (**b**) coexisting chaotic attractors with $a = 3.7$, (**c**) coexisting periodic attractors with $a = 4.051$ and (**d**) coexisting chaotic attractors with $a = 15$.

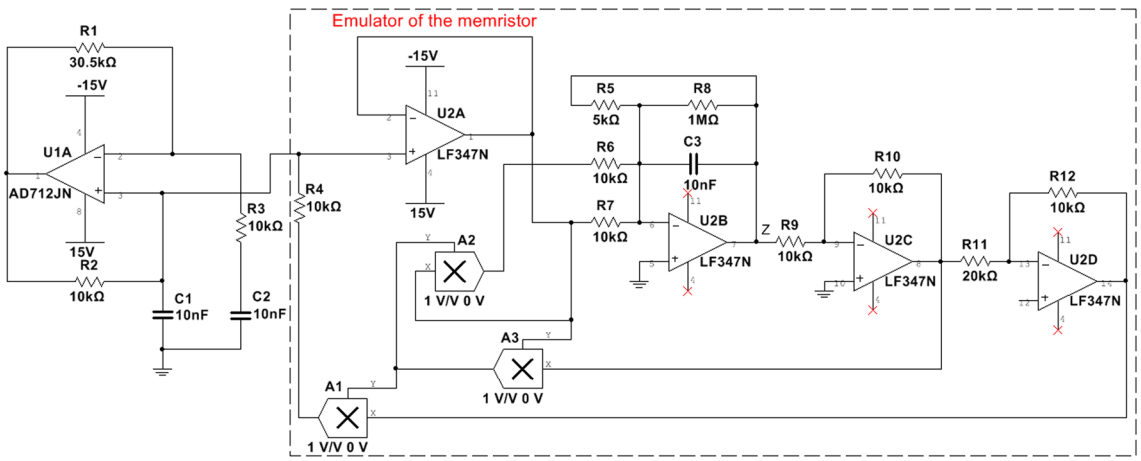

Figure 19. Circuit schematic of realising the system.

with the corresponding constants of motion

$$H(x) = z, \quad C(x) = (a/2)x^2 + (a/2)y^2,$$

whose relation is $g = \nabla H \times \nabla C$. By employing this integrable deformation method, and introducing the deformation functions α and β, the integrable deformation of the memristive Wien-bridge system is

$$\begin{cases} \dfrac{\mathrm{d}x}{\mathrm{d}t} = (ax - by) - (1 + cz^2)x \\ \qquad -\dfrac{\partial\beta}{\partial y} - ay\dfrac{\partial\alpha}{\partial z} + \dfrac{\partial\alpha}{\partial y}\dfrac{\partial\beta}{\partial z} - \dfrac{\partial\alpha}{\partial z}\dfrac{\partial\beta}{\partial y}, \\ \dfrac{\mathrm{d}y}{\mathrm{d}t} = ax - by + \dfrac{\partial\beta}{\partial x} + ax\dfrac{\partial\alpha}{\partial z} - \dfrac{\partial\alpha}{\partial x}\dfrac{\partial\beta}{\partial z} + \dfrac{\partial\alpha}{\partial z}\dfrac{\partial\beta}{\partial x}, \\ \dfrac{\mathrm{d}z}{\mathrm{d}t} = -x - hz + x^2 z + by\dfrac{\partial\alpha}{\partial x} - ax\dfrac{\partial\alpha}{\partial y} \\ \qquad +\dfrac{\partial\alpha}{\partial x}\dfrac{\partial\beta}{\partial y} - \dfrac{\partial\alpha}{\partial y}\dfrac{\partial\beta}{\partial x}. \end{cases} \tag{17}$$

We choose $\alpha = (g/3a)z^3$ and $\beta = 0$ so that the deformed system is symmetrical about the original point. The integrable deformation of system (5) is obtained as

$$\begin{cases} \dfrac{\mathrm{d}x}{\mathrm{d}t} = (ax - by) - (1 + cz^2)x - gyz^2, \\ \dfrac{\mathrm{d}y}{\mathrm{d}t} = ax - by + gxz^2, \\ \dfrac{\mathrm{d}z}{\mathrm{d}t} = -x - hz + x^2z. \end{cases} \tag{18}$$

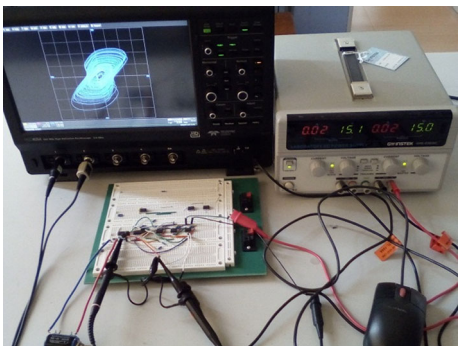

Figure 20. Experimental set-up of the memristive Wien-bridge circuit.

To highlight the multistability of the deformed system, some phase portraits of the coexisting attractors are shown in figure 18, where the parameter a is varied, whereas the other parameters are fixed as $b = 2$, $c = 4.5$, $g = 1$ and $h = 0.4$, and the initial conditions are selected as $(0, 1, 0)$ and $(0, -1, 0)$. In figure 18, coexisting quasiperiodic attractors are observed at $a = 3.28$, coexisting periodic attractors at $a = 4.051$ and two kinds of coexisting chaotic attractors at $a = 3.7, 15$. Moreover, two coexisting chaotic attractors shown as figure 18d are chaotic bursting, and are symmetrical about the original point. Therefore, the deformed system still has multiple types of coexisting attractors with appropriate parameters.

5. Circuit design and experimental results

This chaotic system can be realised via the analogue circuit. For circuit realisation, the time constant which is often called the time scale factor should be taken into account since it influences the frequency and the spectrum of chaotic signal. It is very important to choose

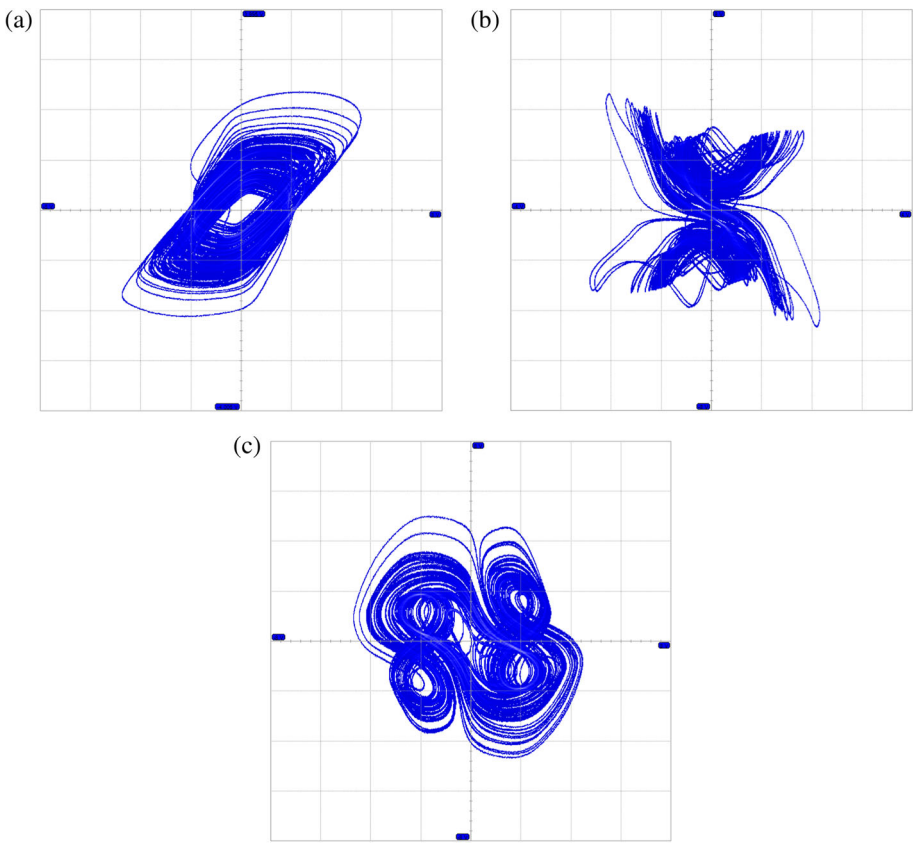

Figure 21. Experimental results of the chaotic system: (**a**) x–y phase diagram, (**b**) y–z phase diagram and (**c**) z–x phase diagram.

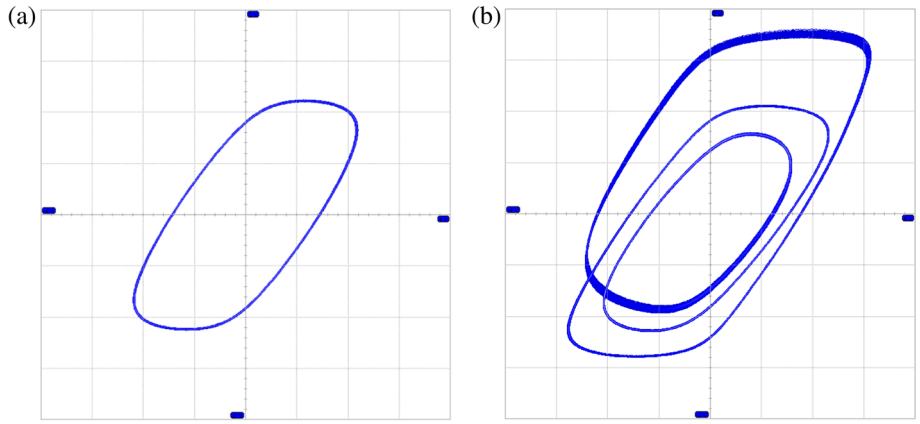

Figure 22. Experimental results of the memristive system: (**a**) period-1 phase diagram and (**b**) period-3 phase diagram.

a suitable time scale factor for easy observation. When the time scale factor K is introduced into eq. (5), and the parameters are chosen as $b = 1$, $c = 0.5$ and $h = 2$, then eq. (5) is rewritten as

$$\begin{cases} \dfrac{\mathrm{d}x}{\mathrm{d}t} = K(ax - y) - K(1 + 0.5z^2)x, \\ \dfrac{\mathrm{d}y}{\mathrm{d}t} = K(ax - y), \\ \dfrac{\mathrm{d}z}{\mathrm{d}t} = -K(x + 2z - x^2 z). \end{cases} \tag{19}$$

If the memristor in the third-order Wien-bridge chaotic system is replaced with its equivalent circuit, and the time-scale factor is chosen as $K = 10{,}000$, the circuit is designed as shown in figure 19, whose state equations are expressed as

$$\begin{cases} \dfrac{\mathrm{d}v_1}{\mathrm{d}t} = \dfrac{(R_1/R_2)v_1 - v_2}{R_3 C_1} - \dfrac{1}{R_4 C_1}\left(1 + \dfrac{R_{12}}{R_{11}}z^2\right)v_1, \\ \dfrac{\mathrm{d}v_2}{\mathrm{d}t} = \dfrac{(R_1/R_2)v_1 - v_2}{R_3 C_2}, \\ \dfrac{\mathrm{d}z}{\mathrm{d}t} = \dfrac{1}{R_7 C_3}\left(-v_1 - \dfrac{R_7}{R_5}z + \dfrac{R_7}{R_6}v_1^2 z\right). \end{cases} \tag{20}$$

For the parameters $a = 3.05$, $b = 1$, $c = 0.5$ and $h = 2$, the values of all the components are taken as shown in figure 19, specifically, $C_1 = C_2 = C_3 = 10$ nF, $R_1 = 30.5\ \mathrm{k\Omega}$, $R_2 = R_3 = R_4 = R_6 = R_7 = R_9 = R_{10} = R_{12} = 10\ \mathrm{k\Omega}$, $R_5 = 5\ \mathrm{k\Omega}$, $R_8 = 1\ \mathrm{M\Omega}$, $R_{11} = 20\ \mathrm{k\Omega}$. The multipliers A_1, A_2 and A_3 in figure 18 are realised by the low cost AD633. By employing the experimental set-up shown in figure 20, the experimental chaotic attractors shown in figure 21 can be obtained, which are captured by the digital oscilloscope. If we vary the value of R_2, the period-1 and period-3 orbits can be observed as shown in figure 22. The circuital experimental results are consistent with the results of numerical simulation.

6. Conclusion

This paper proposes a passive memristor, and designs its equivalent circuit to investigate its fingerprints. Based on the memristor and a non-classical Wien bridge, a third chaotic system without inductive element is constructed, which can produce chaotic multiscroll attractors. Stability analysis shows that it has a unique equilibrium and is symmetrical about the original point. By employing nonlinear analysis tools, the complex nonlinear phenomena of this system are demonstrated, which include coexisting bifurcation modes, coexisting attractors, controllable scroll number, antimonotonicity and transient chaotic bursting. If the initial conditions are symmetric, the coexisting bifurcation modes and the coexistence of periodic, quasiperiodic and chaotic attractors are depicted. Furthermore, the system can generate different scroll attractors by changing the parameters and the initial conditions. More interestingly, the symmetric chaotic bursting of the system is transient, relating to symmetric Hopf–Hopf bifurcation. Then, by using the integrable deformation method, the integrable deformation of the memristive Wien-bridge system is constructed, which can generate multiple types of coexisting attractors. Finally, the third-order Wien-bridge circuit is implemented by replacing the memristor model with its equivalent circuit, and the circuital experiment is performed. The experimental results are consistent with the theoretical analysis. This memristor-based Wien-bridge circuit can be used in the generation of complex pseudosequences for various information encryptions,

such as secret communications, digital watermarking, digital signature and so on.

Acknowledgements

This work was supported by the National Natural Science Foundation of China (Grant Nos 61771176 and 61271064), the Natural Science Foundations of Fujian Province (Grant No. 2016J01761) and the Natural Science Foundation of Zhejiang Province (Grant No. LY18F010012).

References

[1] L O Chua, *IEEE Trans. Circuit Theory* **18**, 507 (1971)
[2] D B Strukov, G S Snider, D R Stewart and R S Williams, *Nature* **453**, 80 (2008)
[3] F Gul and H Efeoglu, *Ceram. Int.* **43**, 10770 (2017)
[4] B J Murdoch, D G McCulloch, R Ganesan, D McKenzie, M M M Bilek and J G Partridge, *Appl. Phys. Lett.* **108**, 143504 (2016)
[5] F B Fauzi, R Othman and M A Mohamed, *Mater. Trans.* **56**, 1302 (2015)
[6] A Kumar, M Das, V Garg, B Sengar, T M Htay, S Kumar, A Kranti and S Mukherjee, *Appl. Phys. Lett.* **110**, 253509 (2017)
[7] P Rabbani, R Dehghani and N Shahpari, *Microelectron. J.* **46**, 1283 (2015)
[8] S Kumar, J P Strachan and R S Williams, *Nature* **548**, 318 (2017)
[9] M Lv and J Ma, *Neurocomputing* **205**, 375 (2016)
[10] C H Wang, H Xia and L Zhou, *Pramana – J. Phys.* **88**: 34 (2017)
[11] M Itoh and L O Chua, *Int. J. Bifurc. Chaos* **18**, 3183 (2008)
[12] I Vourkas and G C Sirakoulis, *IEEE Circ. Syst. Mag.* **16**, 15 (2016)
[13] Z J Li and Y C Zeng, *J. Electron. Inf. Technol.* **36**, 88 (2014)
[14] Q Yu, B C Bao, F W Hu, Q Xu, M Chen and J Wang, *Acta Phys. Sin.* **63**, 240505 (2014)
[15] H G Wu, B C Bao, Z Liu, Q Xu and P Jiang, *Nonlinear Dyn.* **83**, 893 (2016)
[16] X L Ye, J Mou, C F Luo and Z S Wang, *Nonlinear Dyn.* **92**, 923 (2018)
[17] B C Bao, P Y Wu, H Bao, H G Wu, X Zhang and M Chen, *Chaos Solitons Fractals* **109**, 146 (2018)
[18] L O Chua and S M Kang, *Proc. IEEE* **64**, 209 (1976)
[19] M Chen, M Y Li, Q Yu, B C Bao, Q Xu and J Wang, *Nonlinear Dyn.* **81**, 215 (2015)
[20] G Y Wang, F Yuan, G R Chen and Y Zhang, *Chaos* **28**, 013125 (2018)
[21] B C Bao, F W Hu, M Chen, Q Xu and Y J Yu, *Int. J. Bifurc. Chaos* **25**, 1550075 (2015)
[22] J Kengne, A Nguomkam Negou and D Tchiotsop, *Nonlinear Dyn.* **88**, 2589 (2017)
[23] L Zhou, C H Wang, X Zhang and W Yao, *Int. J. Bifurc. Chaos* **28**, 1850050 (2018)
[24] K E Chlouverakis and M J Adams, *IEEE J. Sel. Top. Quant. Electron.* **12**, 398 (2006)
[25] M Deschênes, J P Roy and M Steriade, *Brain Res.* **239**, 289 (1982)
[26] R S K Wong and D A Prince, *J. Neurophysiol.* **45**, 86 (1981)
[27] N H Alombah, H Fotsin and K Romanic, *Int. J. Bifurc. Chaos* **27**, 1750067 (2017)
[28] Y Q Xing, X K Chen, Z D Zhang and Q S Bi, *Acta Phys. Sin.* **65**, 090501 (2016)
[29] B C Bao, P Y Wu, H Bao, M Chen and Q Xu, *Electron. Lett.* **53**, 1104 (2017)
[30] X J Han, Y Yu and C Zhang, *Nonlinear Dyn.* **88**, 2889 (2017)
[31] W Teka, J Tabak and R Bertram, *Chaos* **22**, 1288 (2012)
[32] C Lăzureanu, *Int. J. Bifurc. Chaos* **28**, 1850066 (2018)